

Article

# Studies on Dynamic Properties of Ultracapacitors Using Infinite r–C Chain Equivalent Circuit and Reverse Fourier Transform

Shailendra Rajput <sup>1</sup>, Alon Kuperman <sup>2</sup>, Asher Yahalom <sup>1</sup> and Moshe Averbukh <sup>1,\*</sup>

<sup>1</sup> Department of Electrical/Electronic Engineering, Ariel University, Ariel 40700, Israel; shailendrara@ariel.ac.il (S.R.); asya@ariel.ac.il (A.Y.)

<sup>2</sup> School of Electrical & Computer Engineering, Ben-Gurion University of the Negev, Beer-Sheva 8410501, Israel; alonk@bgu.ac.il

\* Correspondence: mosheav@ariel.ac.il; Tel.: +972-528-814-120

Received: 29 July 2020; Accepted: 3 September 2020; Published: 4 September 2020



**Abstract:** The specific power storage capabilities of double-layer ultracapacitors are receiving significant attention from engineers and scientific researchers. Nevertheless, their dynamic behavior should be studied to improve the performance and for efficient applications in electrical devices. This article presents an infinite resistor–capacitor (r–C) chain-based mathematical model for the analysis of double layer ultracapacitors. The internal resistance and capacitance were measured for repetitive charging and discharging cycles. The magnitudes of internal resistance and capacitance showed approximately  $\pm 10\%$  changes for charge-discharge processes. Electrochemical impedance spectroscopy investigations revealed that the impedance of a double-layer ultracapacitor does not change significantly in the temperature range of ( $-30\text{ }^{\circ}\text{C}$  to  $+30\text{ }^{\circ}\text{C}$ ) and voltage range of ( $0.3376\text{--}2.736\text{ V}$ ). The analysis of impedance data using the proposed mathematical model showed good agreement between the experimental and theoretical data. The dynamic behavior of the ultracapacitor was successfully represented by utilizing the proposed infinite r–C chains equivalent circuit, and the reverse Fourier transform analysis. The r–C electrical equivalent circuit was also analyzed using the PSIM simulation software to study the dynamic behavior of ultracapacitor parameters. The simulation study yields an excellent agreement between the experimental and calculated voltage characteristics for repetitive charging-discharging processes.

**Keywords:** ultracapacitor; equivalent circuit; Fourier transform; internal resistance

## 1. Introduction

Modern technologies such as portable electronic devices, electrical transportation, communication systems, and smart medical equipment need efficient energy storage systems [1,2]. Electrical energy storage devices are also used for smart grid control, grid stability, and peak-power saving as well as for frequency and voltage regulation [3–5]. Electricity generated from renewable sources (e.g., solar power, wind energy) can hardly deliver an immediate response to demand because of fluctuating power supply [6–8]. Hence, it has been suggested to preserve the harvested electrical energy for future requirements. The present status of electrical energy storage technologies is quite far away from the needed demand. These circumstances motivate us to continue scientific research for the improvement in the parameters of existing storage devices and to develop new storage machinery.

Currently, ultracapacitors (UCs) are considered as an efficient energy storage system for electrical devices [9]. Electric double-layer capacitors (EDLCs) or symmetric double-layer UCs have attracted attention as plausible electrical energy storage devices [10–14]. EDLCs are a complex of two identical porous electrodes, electrolytic solution, and a separator, which is used as an ion conductor. The negative

electrode attracts the cations during the charging process, and the anions are collected at the pores of the positive plate. The EDLCs are characterized by longer life cycle due to the absence of chemical reactions, efficient charge-discharge cycles, ability to discharge at higher current density, fast charging-discharging ability, and the lack of heavy metals, which make the device environmentally friendly [11,14]. The increasing popularity of UCs has been directed toward a better understanding of dynamic behavior and ultimately improved performance. The parameters responsible for the dynamic behavior of UCs have not been studied for the applicable range. In very recent work, we studied the dynamic behavior of a double-layer UC [13]. The capacitance remained nearly constant for a wide range of temperatures (+25 °C to −40 °C), but the internal resistance increased ~1.5 times as the temperature decreased to −40 °C [13]. The equivalent electrical circuit models are required to simulate the device parameters for the development and design of electrical appliances. Previously, different types of equivalent circuit models have been proposed in order to understand the dynamic characteristics of UCs [13,15–20]. Importantly, the electrochemical analysis-based modeling approaches have also been employed to study the performance of UCs [21–24].

A mathematical model should demonstrate model precision, robustness, and ease of application in the well-known software platforms (e.g., MATLAB and others). The functionality of UCs is defined by the movement of charged particles (ions) from positive to negative electrodes in the electrolyte. Hence, the correct description of UCs should be based on partial differential equations (PDE). These equations have to describe the continuum flow of ions, which determine the internal resistance and the capacitance of UC. In the electrolyte, the particle movement is related to the diffusion of ions, which is linearly dependent on the concentration difference in adjacent points of a space. The electrical potential describes the charge distributions in the electrolyte, and electrical resistance defines the diffusion movement of ions. Thus, this information should be used to fix the constraints of the equivalent electrical circuit and to characterize the internal resistance and capacitance. In previous studies, this principle is employed to design an equivalent circuit using a finite number of resistors and capacitors [15]. However, the application of a finite number of resistances and capacitances cannot describe UC parameters with high precision. The requirement to simplify the equivalent circuit prevents the use of a significant number of elements. Moreover, the complicated equivalent circuits create substantial mathematical difficulties to determine the magnitudes of equivalent electrical components correctly. Several artificial mathematical operators (fractional impedance [16], Warburg impedance [25], and constant phase element [26]) have been employed to analyze the equivalent circuit. Previous studies did not describe the precise physical phenomena responsible for the electrical properties of UCs. As a result, these equivalent circuits require permanent matching of circuit parameters depending on applied voltage and current. These methods could not explain exact changes in the UC parameters during their functionality since equivalent circuits do not have a rigorous physical base. In a previous article, we proposed that the infinite  $r$ - $C$  chains-based equivalent circuit model could describe the behavior of double layer UCs [13]. The multibranch  $r$ - $C$  circuit modeling approach was also studied by other researchers [27–33]. The frequency-domain models comprise the best overall performance in terms of complexity, correctness, and robustness [31–33]. Logerais et al. proposed the multibranch  $r$ - $C$  circuit model for the analysis of UC [28], but the proposed model did not provide rigorous closed-form analytical solutions and did not consider the inductance of connecting cables and electrodes. Navarro et al. considered the inductance of connecting cables and an infinite number of  $r$ - $C$  chains. However, the reverse Fourier transform can be difficult to apply for the prediction of voltage alterations during charge-discharge due to the lack of a closed-form analytical solution.

This work aimed to study the dynamic behavior of symmetric double layer UC and develop an adequate equivalent circuit model. The novelty of the proposed work was the application of the reverse Fourier transforms to get a time-domain response of UC parameters such as voltage and current. The reverse Fourier transforms analysis was based on the rigorous analytical solution for the frequency-domain impedance spectroscopy. The rest of this paper is organized as follows.

First, the internal resistance and capacitance are measured for repetitive charge-discharge cycles. Second, the impedance, which includes reactance and resistance, is measured at different applied voltage and temperatures using electrochemical impedance spectroscopy (EIS). Third, the impedance data are analyzed using an infinite r-C chain equivalent circuit model. Fourth, dynamic parameters of UC are represented using the reverse Fourier transform analysis. Finally, the proposed equivalent circuit model is simulated using the PSIM simulating package.

## 2. Experimental Studies

### 2.1. Experimental Setup

The dynamic behavior of symmetric double-layer UC (BCAP3400: 3400 F, 2.85 V [34]) was investigated using the electrochemical impedance spectroscopy (EIS), and repetitive charge-discharge cycles. Figure 1a,b demonstrate the experimental setups, and detailed descriptions of experimental setups were discussed in our previous article [13]. For charge-discharge cycle experiments, a charge/discharge system controller [35], regulated DC power supply [36], electronic load [37], and midi-logger GL900 [38] were used. A constant repetitive pulsed current (50 A) was applied for both charge-discharge cycles. The constant current was applied for two seconds, with an interval of two seconds. The internal resistance and capacitance were calculated using the typical voltage vs. time curve for the discharging process [13]. The EIS investigations were performed using the EchemLab XM potentiostat-galvanostat analyzer [39] and Tenney temperature test chamber [40]. The EIS experiments were performed with an AC current of 1 A (rms) and frequencies of 1 Hz–1 kHz.

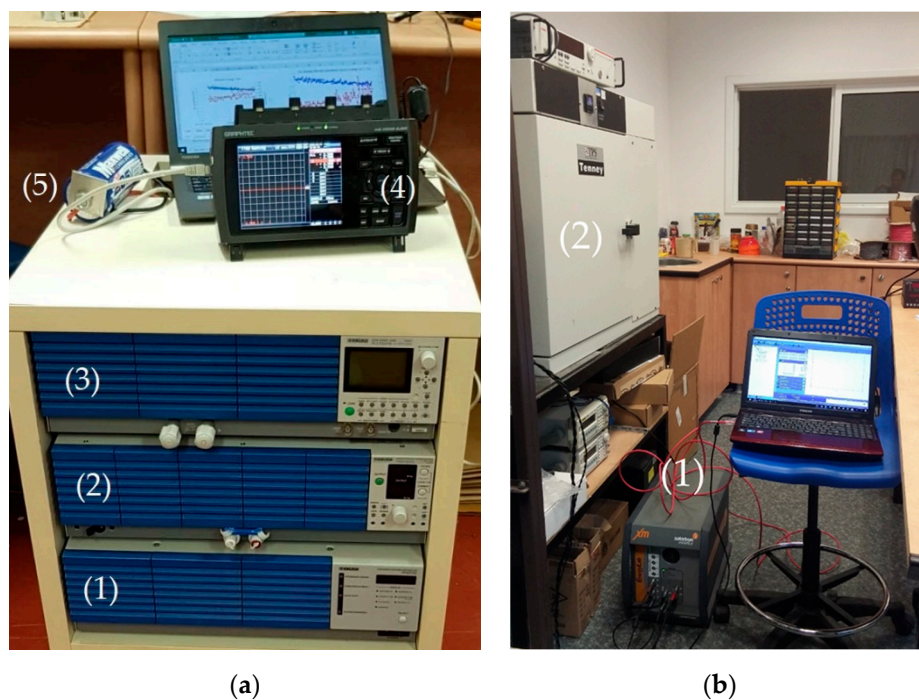


**Figure 1.** (a) Experimental setup for the charge-discharge cycles (1-charge/discharge system controller, 2-regulated DC power supply, 3-electronic load unit, 4-midi-logger, and 5-capacitor). (b) Experimental setup for the EIS measurement (1-Potentiostat-galvanostat, and 2-Tenneytemperature test chamber).

### 2.2. Results

Figure 2 demonstrates the internal resistance ( $R_{int}$ ) and capacitance ( $C$ ) as a function of voltage at a constant current of 50 A. Both the parameters showed approximately  $\pm 10\%$  changes for charge/discharge cycles. Similar outcomes were also observed for an applied current of 20 A and 75 A [13]. It was also noticed that both parameters slightly upsurged as the capacitor voltage enhanced from minimum to

maximum. Importantly, the tendency of UC capacitance during charge/discharge cycles was identical to the internal resistance.

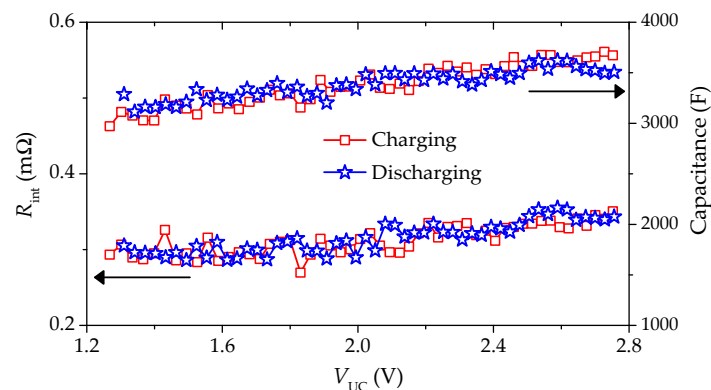


**Figure 2.** Internal resistance and capacitance of symmetric double-layer UC measured at a constant current of 50 A for charge-discharge cycles.

Figure 3a demonstrates the impedance ( $|Z|$ ) of the double layer UC at different temperatures for constant voltage of  $\sim 2.5$  V and frequency range of 1 Hz–100 kHz. Figure 3b shows the impedance ( $|Z|$ ) for different voltages (0.3376–2.736 V) and frequencies of 1 Hz–100 kHz at constant temperature ( $15^\circ\text{C}$ ). The phase impedance of the double-layer UC is shown in Figure 4. The impedance and phase values remained almost constant for different working temperatures ( $-30^\circ\text{C}$  to  $+30^\circ\text{C}$ ). These parameters also remain unchanged for different voltage magnitudes of 0.3376–2.736 V.

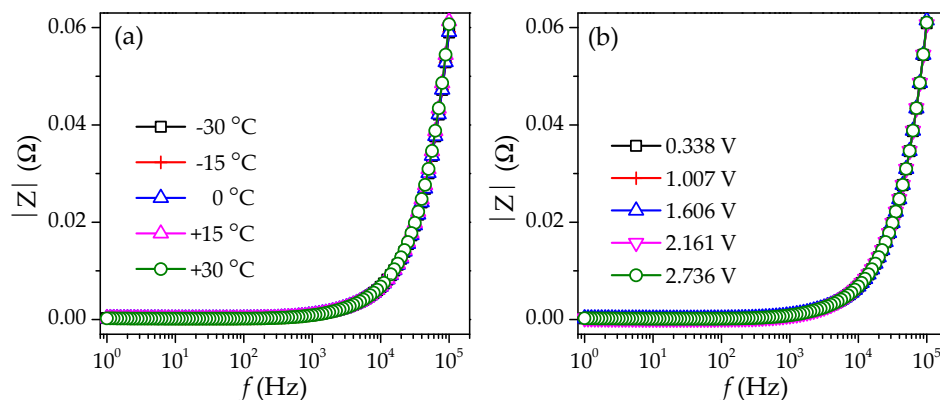


**Figure 3.** Module impedance ( $|Z|$ ) as a function of frequency (a) at different temperatures for constant voltage ( $\sim 2.5$  V), and (b) at different voltages for a constant temperature of  $15^\circ\text{C}$ .

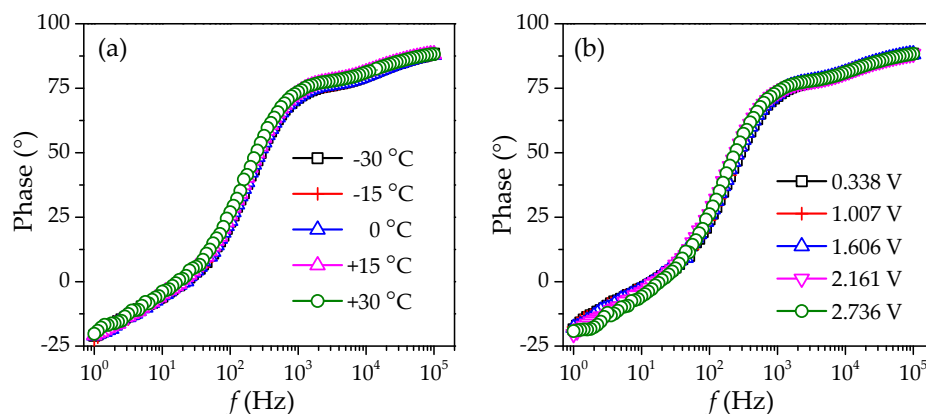


**Figure 4.** Phase ( $\theta$ ) of Z as a function of frequency (a) at different temperatures for constant voltage ( $\sim 2.5$  V) and (b) at different voltages for a constant temperature of  $15^\circ\text{C}$ .

### 3. Equivalent Circuit Development

#### 3.1. Mathematical Model

The equivalent electrical circuit for the analysis of UC was developed by employing a ladder of infinite r–C chains. This approach takes into account the real physical nature of charge movement in the electrolyte. Additionally, it provides high precision of the output UC parameters, however, without the application of PDE. Figure 5 shows the schematic of the proposed infinite r–C chains based equivalent circuit model. The resistor (r) models the resistance of diffusion movement, and consequently, the ohmic loss, which is termed as a real part of equivalent impedance. The element ‘C’ simulates the distribution of space charge in the electrolyte and thus the capacitance of UC. For the mathematical analysis, it was assumed that the r–C chains exhibit similar impedance (Z) as the input one.

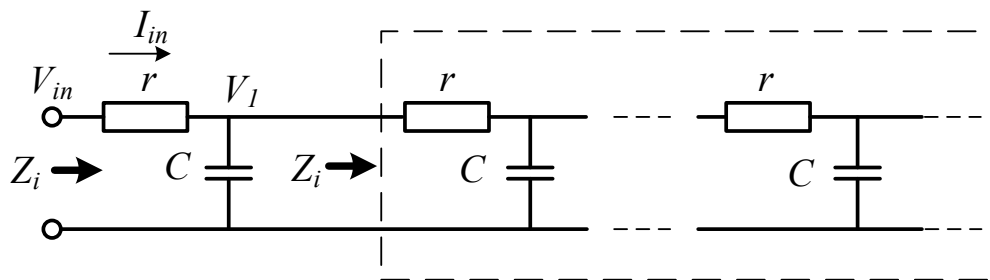


**Figure 5.** Infinite r–C chains based equivalent circuit of a capacitor (r: resistor, C: capacitor, Z<sub>i</sub>: input impedance, V<sub>in</sub>: input voltage, I<sub>in</sub>: input current).

In our previous work, the infinite r–C chain-based equivalent circuit of the UCs was proposed and discussed [13]. The resistance (R) and reactance (X) of this equivalent circuit can be expressed as:

$$R = \frac{1}{2} \left( r + \sqrt{r^2 + 4X^2} \right). \tag{1}$$

$$X = -\sqrt{\frac{-r^2 + \sqrt{r^4 + \left(\frac{4r}{\omega C}\right)^2}}{8}} = -\frac{r}{2\sqrt{2}} \sqrt{\sqrt{1 + \left(\frac{4}{\omega r C}\right)^2} - 1}. \tag{2}$$

Equations (1) and (2) represent the Fourier transform of internal impedance. If the equivalent capacitance is very large (~100–1000 F), then a relatively small inductivity (~10 nH) of connecting cables and electrodes plays a significant role in the measurement of reactance. Hereafter, the component for the inductivity of cables should be included in the equivalent circuit (Figure 6).

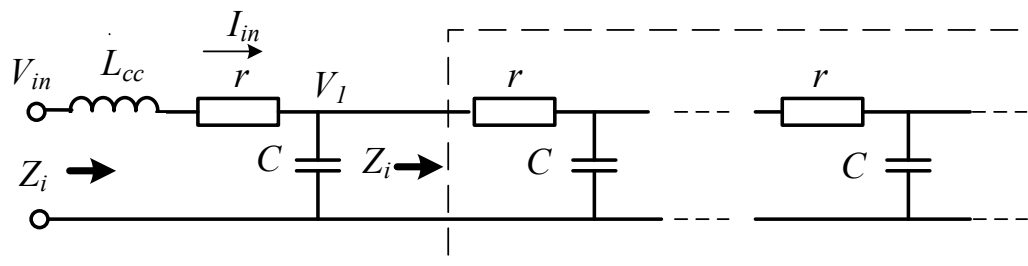


**Figure 6.** Modified equivalent circuit of the ultracapacitor. The component, L<sub>cc</sub>, represents the inductivity of connection wires.

According to the modified equivalent circuit, the total reactance ( $X_T$ ) is written as:

$$X_T = \frac{r}{2} \left( \frac{2\omega L_{cc}}{r} - \frac{1}{\sqrt{2}} \sqrt{\sqrt{1 + \left(\frac{4}{\omega r C}\right)^2} - 1} \right). \quad (3)$$

Inserting Equation (3) into Equation (1) gives the resistance R:

$$R = \frac{r}{2} \left( 1 + \sqrt{1 + \left( \frac{2\omega L_{cc}}{r} - \frac{1}{\sqrt{2}} \sqrt{\sqrt{1 + \left(\frac{4}{\omega r C}\right)^2} - 1} \right)^2} \right). \quad (4)$$

Figure 7 demonstrates the comparison between experimental and calculated EIS data. Equations (3) and (4) are employed for the simulation, and the least-mean squares approach was applied for the theoretical fitting. The coefficient of determination ( $\chi^2$ ) decides the criterion of the proximity between the theoretical and experimental output. This large value of  $\chi^2$  ( $\sim 0.992$ ) proved the accuracy of the proposed method, although this analysis was performed for the EIS data measured at a temperature of 15 °C,  $V_{UC}$  of 2.736 V, and AC current of 1.4 A. However, this model was valid for data measured at different temperatures and voltages (Figure 3).

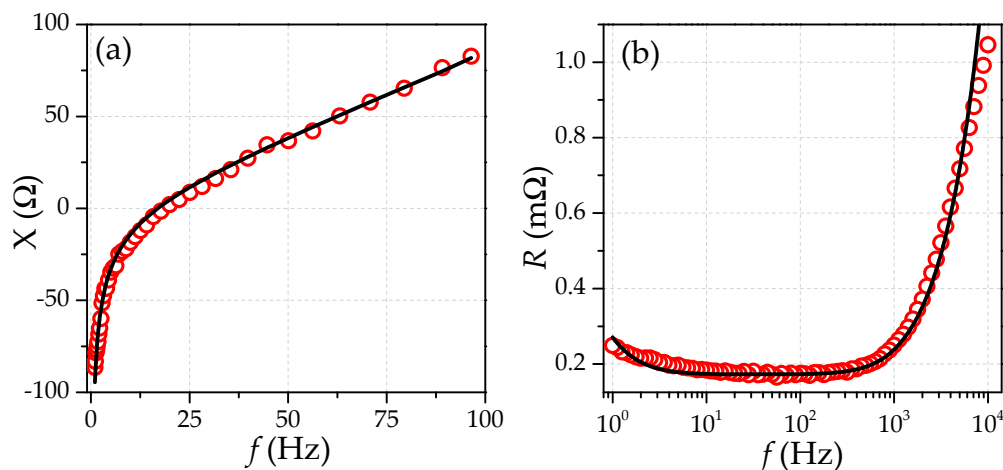


**Figure 7.** Simulated and measured EIS data of symmetric double-layer UC (a) reactance, (b) resistance.

The internal resistance and capacitance exhibited relatively small change ( $\pm 10$ – $15\%$ ) for the applicable voltage range (Figure 2). Hence, the constant parameter representation was considered for the calculation of equivalent circuit parameters. The proposed model should be modified accordingly, if the voltage and current parameters are altered significantly.

### 3.2. Representation of Dynamic UC Parameters Using Reverse Fourier Transform

The equivalent circuit and obtained parameters ( $r$  and  $C$ ) can be utilized to determine the voltage and current parameters of UC for different working conditions. For this purpose, a reverse Fourier transformation was applied. Let us consider that current ( $I_{in}$ ) is applied as input for the equivalent circuit (Figure 5). Using nodal analysis, the voltage ( $V_1$ ) is expressed as:

$$V_1 \left( j\omega C + \frac{1}{Z} \right) = I_{in} \Rightarrow V_1 = \frac{I_{in}}{j\omega C + \frac{1}{Z}} \quad (5)$$

where  $V_1$  and  $Z$  are assumed as complex variables. The solution of the following Fourier integral is needed to restore the capacitor voltage [41]:

$$V_1(t) = \frac{2}{\pi} \int_0^{\infty} \frac{R(\omega) \sin(\omega t)}{\omega} d\omega \quad (6)$$

where  $R(\omega)$  is the real part of the Fourier transform of  $V_1$  (Equation (4)). The input voltage ( $V_{in}$ ) can be calculated:

$$V_{in} = V_1 + \Delta V_r = V_1 + I_{in}r \quad (7)$$

where  $\Delta V_r = I_{in}r$  is the voltage drop at the resistance  $r$ . The numerical approaches can only solve the integral (6) because of its irrational form. First, the real part of the impedance is obtained using the specific values of  $r$  and  $C$  following the expression (4). Second, the real part of  $Z$  is substituted to the integral (6), which is numerically solved for the required series of time ( $t_0$ – $t_{max}$ ) and time resolution ( $\Delta t$ ). Using the proposed model and EIS data, the equivalent circuit parameters can be calculated as  $r = 0.1 \text{ m}\Omega$ ,  $C = 800 \text{ F}$ . The voltage of UC for charge-discharge processes was simulated for the constant input current of 20 A. The simulated and measured dynamic characteristics of UC for both charge-discharge cycles are demonstrated in Figure 8. The numerical analysis of Fourier integral provides the expected output for charging-discharging processes. The theoretical analysis was consistent with the experimental one, which approves the transverse Fourier transformation for the restoration of UC dynamic behavior.

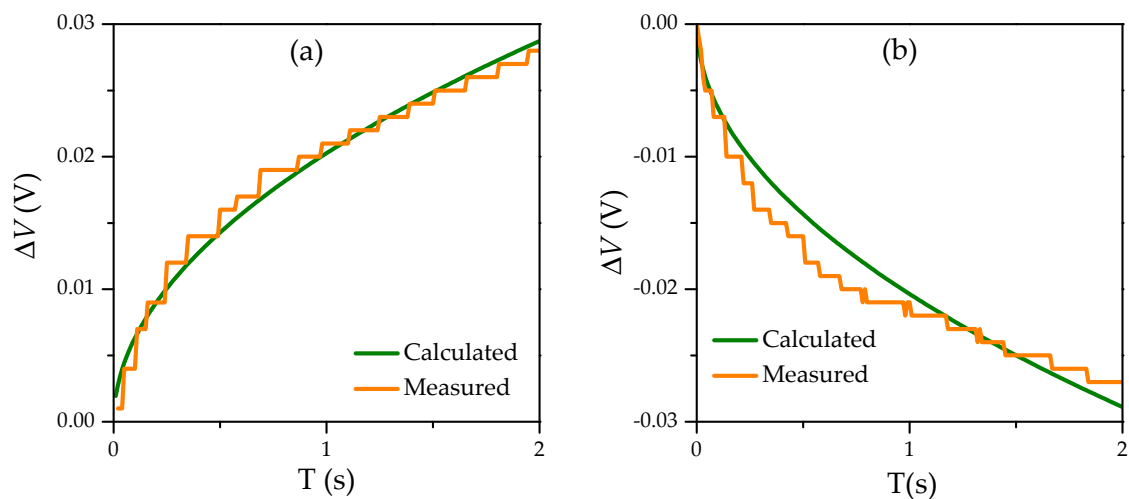


**Figure 8.** Representation of dynamic behavior of UC voltage using reverse Fourier transform (a) charging process, (b) discharging process. The UC characteristics are measured at constant input current of 20 A and temperature of 30 °C.

The restoration of parameters can also be achieved by the integral given below:

$$V(t) = \frac{1}{2\pi} \int_{-\infty}^{\infty} F(\omega) e^{j\omega t} d\omega \quad (8)$$

where  $F(\omega)$  is the Fourier transform of the input current and can be written as:

$$F(\omega) = \int_{-\infty}^{\infty} V(t) e^{-j\omega t} dt \quad (9)$$

Generally,  $F(\omega)$  is a complex variable and contains real and imaginary parts. The rigorous finite analytical representation of the Fourier transform exists for several functions (e.g., step- and

pulse-function). However, an analytical Fourier formulation could not be presented for each mathematical expression.

#### 4. Equivalent Circuit Model with PSIM Software

The previous section stated that the Fourier reverse transformation could be applied only for a restricted class of mathematical expressions. Hence, simulation of the electrical circuit using appropriate software is a convenient and efficient method. For arbitrary functions, one of the most efficient software is the PSIM simulating package [42].

The equivalent circuit model was developed to simulate the periodic charge-discharge process of UC (Figure 9). The model includes a ladder of ten r-C chains and inductivity of connecting cables. This circuit can be applied for any arbitrary current input function. For example, the galvanostatic measurements can be carried out by applying the AC control signal as the input of a current source. Figure 10 shows the measured and simulated (using proposed model) voltage behavior of the symmetric double layer UC for periodic charging-discharging cycles with a constant current of  $\pm 100$  A, a period of 3 s, and duty-cycle relation of 0.5. The instantaneous deviations of a voltage over its steady-state magnitude were measured. The simulation study yielded an excellent agreement between the experimental and calculated charge-discharge characteristics of UC. The accuracy of such a model lay inside 5–8% of the relative error between the calculated and experimental data.

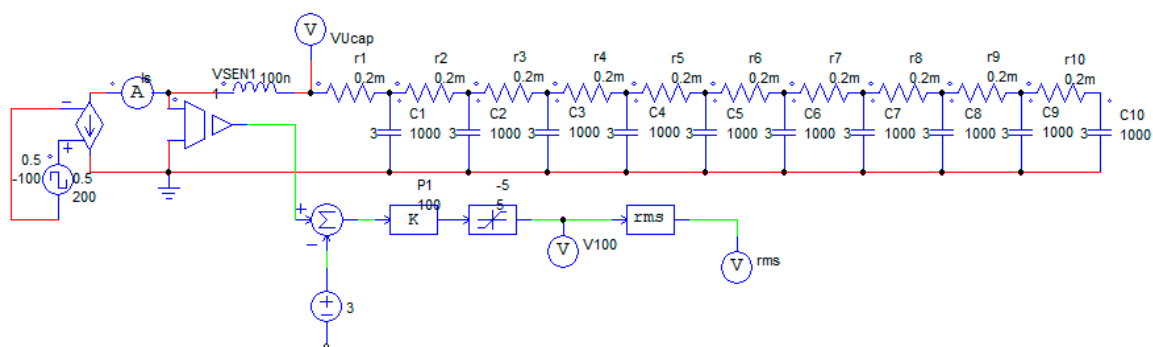


**Figure 9.** Model of the equivalent electrical circuit for the galvanostatic measurement. This model comprises ten r-C chains and includes the inductivity of connecting cables.

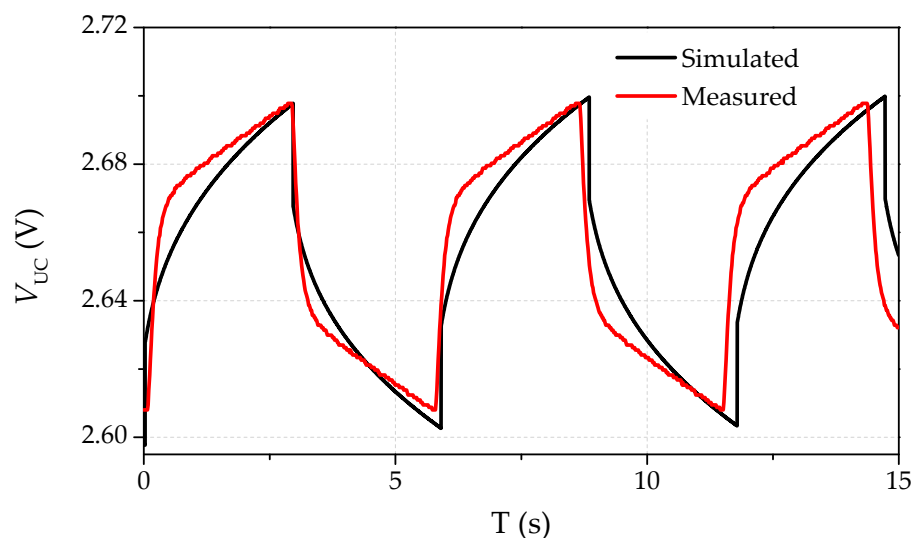


**Figure 10.** The experimental and simulated characteristics of symmetric double layer UC for periodic charging and discharging cycles.

## 5. Discussion

The proposed model can effectively describe the dynamic behavior of UC without the usage of PDEs. This model describes the concentration of ions by an electrical potential, charge diffusive motion by electric current, and diffusion coefficient by electrical resistance. Therefore, the exact physical nature of electrolyte is considered in the proposed mathematical model. The infinite r-C chain-based equivalent circuit exactly describes the behavior of ion movement in the electrolyte and porous electrodes. Moreover, we succeeded in finding a rigorous analytical solution of this model in the closed form. The symmetric double layer UCs are purely electrostatic devices. Hence, no electrochemical (Faradaic) reactions occur on electrodes instead of asymmetrical UCs, where the electrochemical reactions occur in the one compartment of UC. Therefore, the voltage-dependent term (pseudo-capacitance related to Faradaic reactions) is not considered in the model. Some previous studies have considered the voltage-dependent capacitance term for the modeling [33,43]. Rafik et al. claimed that consideration of the voltage-dependent term could improve the modeling precision by 10% more than that of constant term approximation [33]. If the voltage and current deviations are significantly large, then the parameters should be adjusted accordingly. Future works will consider the incorporation of voltage-dependent capacitance term in the infinite r-C chain equivalent circuit. More importantly, this study also approved the principle possibility of applying the reverse Fourier transform on the frequency domain for the description of dynamic behavior. We also want to mention that the finite analytical representation of the Fourier transform cannot be applied for every mathematical expression. Hence, the proposed model was analyzed using simulation software to study the dynamic behavior of UC. The experimental and calculated charge-discharge characteristics displayed good agreement with a relative error of 5–8%. During the modeling, it was noted that a higher number of r-C chains led to higher accuracy in the impedance representation. Last but not least, we want to mention that this article strengthens the usefulness and advantages of the infinite r-C chains-based equivalent circuit.

## 6. Conclusions

The infinite number of r-C chain-based equivalent circuit for a symmetric double-layer UC was evaluated in this work. The dynamic characteristics were studied to authenticate the applicability of the projected equivalent circuit in the practical working conditions. The internal resistance and capacitance values of the ultracapacitor remained relatively constant for the charging-discharging processes despite the current and voltage change in a wide range of parameters. However, the internal resistance is strongly influenced by the working temperature. The possible reason is the decay of the diffusion coefficient at lower temperatures. The EIS studies confirmed that the impedance remained constant for a wide range of applied voltage (0.3376–2.736 V) and temperatures (−30 °C to +30 °C). The reactance was determined by an inductive reactance of a connecting cable, especially for frequencies higher than 100 Hz. Following from the inductive reactance nature, the temperature did not influence it. The UC functionality, periodic, and stochastic phases of the charge-discharge current are recommended to verify using simulation software. An electrical engineer can apply the proposed equivalent circuit to estimate the electrical parameters for the development of energy storage facilities.

**Author Contributions:** Conceptualization, M.A., A.K., and A.Y.; Methodology, M.A. and S.R.; Software, M.A. and S.R.; Formal analysis, M.A., A.K., and A.Y.; Investigation, S.R.; Resources, M.A. and A.Y.; Data curation, S.R. and M.A.; Writing—original draft preparation, S.R. and M.A.; Writing—review and editing, S.R., A.K., A.Y., and M.A.; Supervision, A.Y. and M.A.; Project administration, M.A. All authors have read and agreed to the published version of the manuscript.

**Funding:** This research received no external funding.

**Acknowledgments:** The authors gratefully acknowledge the support of M. Zinigrad (Ariel University), Y. Bernstein (Ariel University), and M. Perl (Wise-Tech. Co.) for the experiments. S. Rajput is thankful to the Israeli Council for Higher Education (CHE) for the fellowship.

**Conflicts of Interest:** The authors declare no conflict of interest.

## References

1. Shtessel, Y.B.; Ghanes, M.; Ashok, R.S. Hydrogen Fuel Cell and Ultracapacitor Based Electric Power System Sliding Mode Control: Electric Vehicle Application. *Energies* **2020**, *13*, 2798. [[CrossRef](#)]
2. Karden, E.; Ploumen, S.; Fricke, B.; Miller, T.; Snyder, K. Energy storage devices for future hybrid electric vehicles. *J. Power Sources* **2007**, *168*, 2–11. [[CrossRef](#)]
3. Wong, L.A.; Ramachandaramurthy, V.K.; Taylor, P.; Ekanayake, J.B.; Walker, S.L.; Padmanaban, S. Review on the optimal placement, sizing and control of an energy storage system in the distribution network. *J. Energy Storage* **2019**, *21*, 489. [[CrossRef](#)]
4. Rajput, S.; Amiel, I.; Sitbon, M.; Aharon, I.; Averbukh, M. Control the Voltage Instabilities of Distribution Lines using Capacitive Reactive Power. *Energies* **2020**, *13*, 875. [[CrossRef](#)]
5. Sorkin, O.; Farber, E.; Averbukh, M. Selecting ultracapacitors for smoothing voltage deviations in local grids fed by transformer with tap-changer and distributed PV facilities. *Electronics* **2019**, *8*, 357. [[CrossRef](#)]
6. Heard, B.P.; Brook, B.W.; Wigley, T.M.; Bradshaw, C.J. Burden of proof: A comprehensive review of the feasibility of 100% renewable-electricity systems. *Renew. Sustain. Energy Rev.* **2017**, *76*, 1122. [[CrossRef](#)]
7. Rajput, S.; Averbukh, M.; Yahalom, A.; Minav, T. An Approval of MPPT Based on PV Cell's Simplified Equivalent Circuit During Fast-Shading Conditions. *Electronics* **2019**, *8*, 1060. [[CrossRef](#)]
8. Kumar, G.V.B.; Sarojini, R.K.; Palanisamy, K.; Padmanaban, S.; Holm-Nielsen, J.B. Large Scale Renewable Energy Integration: Issues and Solutions. *Energies* **2019**, *12*, 1996. [[CrossRef](#)]
9. Averbukh, M.; Lineykin, S.; Kuperman, A. Portable ultracapacitor based power source for emergency starting of internal combustion engines. *IEEE Trans. Power Electron.* **2015**, *30*, 4283–4290. [[CrossRef](#)]
10. Uno, M.; Iwasaki, K.; Hasegawa, K. Series-Parallel Reconfiguration Technique with Voltage Equalization Capability for Electric Double-Layer Capacitor Modules. *Energies* **2019**, *12*, 2741. [[CrossRef](#)]
11. Ito, Y.; Yanagisawa, H.; inventors; Panasonic Intellectual Property Management Co Ltd. assignee. Electrolyte Solution for Electric Double Layer Capacitors, and Electric Double Layer Capacitor. U.S. Patent 10,199,179, 5 February 2019.
12. Teuber, M.; Strautmann, M.; Drillkens, J.; Sauer, D.U. Lifetime and Performance Assessment of Commercial Electric Double-Layer Capacitors Based on Cover Layer Formation. *ACS Appl. Mater. Interfaces* **2019**, *11*, 18313. [[CrossRef](#)]
13. Abetbool, Y.; Rajput, S.; Yahalom, A.; Averbukh, M. Comprehensive Study on Dynamic Parameters of Symmetric and Asymmetric Ultracapacitors. *Electronics* **2019**, *8*, 891. [[CrossRef](#)]
14. Muzaffar, A.; Ahamed, M.B.; Deshmukh, K.; Thirumalai, J. A review on recent advances in hybrid supercapacitors: Design, fabrication and applications. *Renew. Sustain. Energy Rev.* **2019**, *101*, 123. [[CrossRef](#)]
15. Jiya, I.N.; Gurusinge, N.; Gouws, R. Electrical Circuit Modelling of Double Layer Capacitors for Power Electronics and Energy Storage Applications: A Review. *Electronics* **2018**, *7*, 268. [[CrossRef](#)]
16. Guo, J.; Liu, W.; Chu, L.; Zhao, J. Fractional-Order Modeling and Parameter Identification for Ultracapacitors with a New Hybrid SOA Method. *Energies* **2019**, *12*, 4251. [[CrossRef](#)]
17. Skovranek, T.; Macias, M.; Sierociuk, D.; Malesza, W.; Dzielinski, A.; Podlubny, I.; Pocsova, J.; Petras, I. Anomalous diffusion modeling using ultracapacitors in domino ladder circuit. *Microelectron. J.* **2019**, *84*, 136. [[CrossRef](#)]
18. Kang, J.; Wen, J.; Jayaram, S.H.; Yu, A.; Wang, X. Development of an equivalent circuit model for electrochemical double layer capacitors (EDLCs) with distinct electrolytes. *Electrochim. Acta* **2014**, *115*, 587. [[CrossRef](#)]
19. Pozo, B.; Garate, J.I.; Ferreira, S.; Fernandez, I.; de Gorostiza, E.F. Supercapacitor Electro-Mathematical and Machine Learning Modelling for Low Power Applications. *Electronics* **2018**, *7*, 44. [[CrossRef](#)]
20. Song, S.; Zhang, X.; Li, C.; Wang, K.; Sun, X.; Huo, Q.; Wei, T.; Ma, Y. Equivalent circuit models and parameter identification methods for lithium-ion capacitors. *J. Energy Storage* **2019**, *24*, 100762. [[CrossRef](#)]
21. Buller, S.; Karden, E.; Kok, D.; Doncker, R.W.D. Modeling the dynamic behavior of supercapacitors using impedance spectroscopy. *IEEE Trans. Ind. Appl.* **2002**, *38*, 1622. [[CrossRef](#)]
22. Zhang, L.; Hu, X.; Wang, Z.; Sun, F.; Dorrell, D.G. A review of supercapacitor modeling, estimation, and applications: A control/management perspective. *Renew. Sustain. Energy Rev.* **2018**, *81*, 1868–1878. [[CrossRef](#)]

23. Drummond, R.; Zhao, S.; Howey, D.A.; Duncan, S.R. Circuit synthesis of electrochemical supercapacitor models. *J. Energy Storage* **2017**, *10*, 48. [[CrossRef](#)]
24. Yu, A.; Chabot, V.; Zhang, J. *Electrochemical Supercapacitors for Energy Storage and Delivery: Fundamentals and Applications*; CRC Press: Boca Raton, FL, USA, 2017.
25. Barbero, G.; Lelidis, I. Analysis of Warburg's impedance and its equivalent electric circuits. *Phys. Chem. Chem. Phys.* **2017**, *19*, 24934. [[CrossRef](#)] [[PubMed](#)]
26. De Pauli, M.; Gomes, A.M.; Cavalcante, R.L.; Serpa, R.B.; Reis, C.P.; Reis, F.T.; Sartorelli, M.L. Capacitance spectra extracted from EIS by a model-free generalized phase element analysis. *Electrochim. Acta* **2019**, *320*, 134366. [[CrossRef](#)]
27. Belhachemi, F. *Modélisation et Caractérisation des Supercondensateurs à Couche Double Électrique Utilisés en Électronique de Puissance (Doctoral Dissertation)*; National Polytechnic Institute of Lorraine (INPL): Lorraine, France, 2001.
28. Logerais, P.O.; Camara, M.A.; Riou, O.; Djellad, A.; Omeiri, A.; Delaleux, F.; Durastanti, J.F. Modeling of a supercapacitor with a multibranch circuit. *Int. J. Hydrog. Energy* **2015**, *40*, 13725. [[CrossRef](#)]
29. Berrueta, A.; Martin, I.S.; Hernández, A.; Ursúa, A.; Sanchis, P. Electro-thermal modelling of a supercapacitor and experimental validation. *J. Power Sources* **2014**, *259*, 154. [[CrossRef](#)]
30. Belhachemi, F.; Rael, S.; Davat, B. A physical based model of power electric double-layer supercapacitors. In Proceedings of the Conference Record of the 2000 IEEE Industry Applications Conference, Rome, Italy, 8–12 October 2000; pp. 3069–3076.
31. Navarro, G.; Nájera, J.; Torres, J.; Blanco, M.; Santos, M.; Lafoz, M. Development and Experimental Validation of a Supercapacitor Frequency Domain Model for Industrial Energy Applications Considering Dynamic Behaviour at High Frequencies. *Energies* **2020**, *13*, 1156. [[CrossRef](#)]
32. Musolino, V.; Piegari, L.; Tironi, E. New full-frequency-range supercapacitor model with easy identification procedure. *IEEE Trans. Ind. Electron.* **2012**, *60*, 112. [[CrossRef](#)]
33. Rafik, F.; Gualous, H.; Gallay, R.; Crausaz, A.; Berthon, A. Frequency, thermal and voltage supercapacitor characterization and modeling. *J. Power Sources* **2007**, *165*, 928. [[CrossRef](#)]
34. K2 ULTRACAPACITORS: 2.85V/3400F. Available online: [https://www.maxwell.com/images/documents/K2\\_2\\_85V\\_DS\\_3000619EN\\_3\\_.pdf](https://www.maxwell.com/images/documents/K2_2_85V_DS_3000619EN_3_.pdf) (accessed on 7 January 2020).
35. Charge/Discharge System Controller, PFX2532. Available online: <https://www.kikusui.co.jp/en/product/detail.php?IdFamily=0118> (accessed on 19 January 2020).
36. Variable-Switching MultiRange DC Power Supply PWR 1600W. Available online: <https://www.kikusui.co.jp/en/product/detail.php?IdFamily=0064> (accessed on 19 January 2020).
37. Multifunctional DC Electronic Load, PLZ-4W Series. Available online: <https://www.kikusui.co.jp/en/product/detail.php?IdFamily=0011> (accessed on 19 January 2020).
38. Midi Logger GL900. Available online: <http://www.graph-tec.com/instruments/gl900/index.html> (accessed on 27 January 2020).
39. EchemLab XM Potentiostat Galvanostat. Available online: <https://www.ameteksi.com/products/potentiostats/single-channel/apps-xm-series/echemlab-xm-potentiostat-galvanostat> (accessed on 1 March 2020).
40. Lunaire Steady State Testing Chamber. Available online: <https://www.thermalproductsolutions.com/brands/tenney-lunaire-environmental-test-chambers-and-rooms> (accessed on 6 March 2020).
41. Shenkman, A.L.; Zarudi, M. *Circuit Analysis for Power Engineering Handbook*; Springer Science & Business Media: Berlin, Germany, 2012.
42. PSIM-Software for Power Electronics. Available online: <https://powersimtech.com/products/psim/> (accessed on 10 May 2020).
43. Zubietta, L.; Bonert, R. Characterization of double-layer capacitors for power electronics applications. *IEEE Trans. Ind. Appl.* **2000**, *36*, 199. [[CrossRef](#)]

